L-shell shake processes resulting from 1s photoionization in elements $11 \leqslant Z \leqslant 17$

O. Mauron, J.-Cl. Dousse, and J. Hoszowska*
Department of Physics, University of Fribourg, Chemin du Musée 3, CH-1700 Fribourg, Switzerland

J. P. Marques and F. Parente
Centro de Física Atómica e Departamento de Física da Universidade de Lisboa, Avenida Professor Gama Pinto 2, 1649-003 Lisboa, Portugal

M. Polasik
Faculty of Chemistry, Nicholas Copernicus University, Gagarina 7, 87-100 Toruń, Poland
(Received 11 July 2000; published 10 November 2000)

The photoinduced $K\alpha$ x-ray spectra of elements between sodium and chlorine were measured by means of high-resolution crystal diffractometry. The $K\alpha_{1,2}L^{(1)}$ satellites were observed and resolved from the corresponding diagram lines. The probabilities for producing via shake processes $K^{(1)}L^{(1)}$ double-hole states were deduced from the satellite to parent diagram line yield ratios. The results are compared to theoretical sudden approximation predictions. A satisfactory agreement is found except for sodium and chlorine for which our experimental results are markedly underestimated by the calculations.

PACS number(s): 32.30.Rj, 32.80.Fb, 34.50.Fa

I. INTRODUCTION

Atomic inner-shell photoionization is a process in which a single photon can be assumed to interact with a single bound electron. Direct multiple ionization caused by photoionization can be considered as negligibly small but excited atomic states with more than one inner-shell vacancy are, however, frequently observed as a result of photoionization [1]. The observation in K x-ray spectra of satellites emitted when the primary excited states decay proves that processes other than radiationless transitions do contribute to the multiple excitation. In fact, when a sudden change in atomic potential occurs, there exists a probability of an atomic electron to be excited to an unoccupied bound state or to the continuum. These processes are called shake-up and shake-off, respectively. The atomic potential ''seen'' by an electron may change because of a fast removal of another innermost electron or because of a sudden change of nuclear charge due to nuclear decay (α-particle emission, β decay, or electron capture).

Experimental evidence of atomic excitation due to the production of an inner-shell vacancy, through photoionization, electron-impact ionization, and internal conversion, has been established a long time ago in the study of satellite lines or satellite continuum in x-rays and photoelectron spectra [2–4].

Satellite yields observed in photoinduced K x-ray spectra can be assumed to result quasiexclusively from shake processes. Using this assumption we have determined the probabilities for L-shell shake processes following 1s photoionization in the elements comprised between $11 \leqslant Z \leqslant 17$. The L-shell shakeoff plus shakeup probabilities were determined from the measured intensity ratios of the $KL^{(1)}$ satellites to the $KL^{(0)}$ parent diagram lines. All measurements were performed with pure elements, except for chlorine for which two different compounds were employed (NaCl and RbCl). In order to probe the size of chemical effects on the shake probabilities, a pure Na target and a compound NaCl one were used for the measurements of the K x-ray emission spectrum of sodium.

II. EXPERIMENT

A. Experimental method

The L-shell shake probabilities were deduced from the observed $X_{K\alpha L^{(1)}}$:$X_{K\alpha L^{(0)}}$ relative satellite x-ray yields. For the yields $X_{K\alpha L^{(0)}}$ of the diagram lines, we have summed the intensities of the $K\alpha_{1,2}$ transitions and unresolved M satellite structures. Depending on the elements, the complex L satellite structures were fitted with two or three components, the intensities of which were added to get the $X_{K\alpha L^{(1)}}$ yields. From the so-determined relative x-ray yields $X_{K\alpha L^{(1)}}$:$X_{K\alpha L^{(0)}}$, the primary vacancy yield ratios $I_{K\alpha L^{(1)}}$:$I_{K\alpha L^{(0)}}$ were then computed, using simple statistical considerations to account for the L-vacancy rearrangement by intra-atomic electron transitions preceding the K x-ray emission. Finally, the L-shell shake probabilities were calculated from these $I_{K\alpha L^{(1)}}$:$I_{K\alpha L^{(0)}}$ ratios which represent the percentage of KL double-vacancy states relative to K single-vacancy states just after the 1s photoionization of the target atoms.

B. Instrumentation

The measurements of the photoinduced K x-ray spectra were performed at the University of Fribourg by means of a reflecting-type von Hamos curved crystal spectrometer [5]. The main characteristics of this instrument were already presented in several previous papers [1,6,7]. Thus, in the following, only the features specific to the setup used for the present experiment will be discussed.

*Present address: European Synchrotron Radiation Facility, 156 rue des Martyrs, F-38043 Grenoble Cedex, France.

The principal elements of the spectrometer are an x-ray source defined by a rectangular slit, a cylindrically bent crystal, and a position-sensitive detector. The vertical rectangular slit consisted of two juxtaposed Ta pieces 0.3 mm thick and 10 mm high. For all measurements a slit width of 0.2 mm was used. The targets were irradiated with the bremsstrahlung of a Cr x-ray tube. Each target was aligned around a vertical axis so that the angles between the target plane and the irradiation and observation directions were the same. For the Al, Si, P, S, and Cl measurements, the spectrometer was equipped with a 5-cm-wide$\times$10-cm-high$\times$0.3-mm-thick (101) ADP crystal ($2d=10.642$ Å). For Na and Mg a (001) TlAP crystal ($2d=25.900$ Å) was employed. The Bragg-angle domain covered by the von Hamos spectrometer extends from 24.4° to 61.1°. For the ADP and TlAP crystals the corresponding energy intervals are thus comprised for first-order reflections between 1.331 and 2.820 keV, and 0.547 and 1.158 keV, respectively. Both crystals were curved cylindrically to a nominal radius of 25.4 cm. The measurements, however, were performed at a focusing distance of 24.9 cm, for which the best instrumental resolution was obtained. All elements were measured in first order of reflection except Mg which was measured in second order because the $K\alpha$ x-ray spectrum of this element falls exactly in the gap between the energy bandwidths covered by the two crystals.

In the von Hamos slit geometry the instrumental broadening is determined by the slit aperture, precision of the crystal curvature, crystal mosaïcity, and by the spatial resolution of the position-sensitive detector. For the measurements performed with the ADP crystal, the spectrometer resolution varied between 0.37 eV (Al spectrum) and 1.28 eV (Cl spectrum), the slit contribution being 0.23 eV and 0.85 eV, respectively. For the Na and Mg measurements which were performed with the TlAP crystal, the instrumental broadening amounted to 1.20 eV (slit contribution of 0.33 eV included) and 0.64 eV (slit: 0.21 eV), respectively. The better resolution of the Mg measurement is due to the fact that in this case, as mentioned above, the spectrum was observed in second order.

The x rays were recorded with a 27.65-mm-long and 6.9-mm-high charge-coupled-device (CCD) position-sensitive detector, having a depletion depth of 50 μm. The 27-μm pixel resolution of the CCD being many times better than the natural linewidth of the observed transitions, a software binning of four columns was performed in order to obtain higher count rates in the position spectra. Finally the position spectra were calibrated in energy by means of the formulas (3) and (4) given in [5], using the $K\alpha_1$ energies quoted in Ref. [8]. The experimental settings used in the measurements are summarized in Table I.

TABLE I. Experimental settings.

Z	Target	X-ray tube	Acquisition time (s)	Crystal	Reflection order	η_{KL}[a]
11	Na	40 kV 20 mA	60000	TlAP	1	142
11	NaCl	40 kV 20 mA	40000	TlAP	1	109
12	Mg	40 kV 20 mA	12000	TlAP	2	80
13	Al	30 kV 10 mA	8000	ADP	1	57
14	Si	30 kV 10 mA	8000	ADP	1	49
15	P	25 kV 10 mA	6000	ADP	1	37
16	S	40 kV 20 mA	6000	ADP	1	34
17	RbCl	30 kV 15 mA	20000	ADP	1	20
17	NaCl	30 kV 15 mA	6000	ADP	1	23

[a]Parameter describing the photoelectron velocity (see text).

C. Targets

The elemental Na target was prepared by rolling carefully a lump of the soft and extremely reactive metal until a foil with a thickness of about 0.2 mm was attained. The thin foil was then glued on an aluminum backing and brought promptly into the high-vacuum chamber of the spectrometer for the measurements. The Mg and Al targets consisted of thin metallic foils, 0.01 mm and 0.006 mm thick, respectively. The Al foil was mounted on an aluminum frame whereas the Mg target was glued on a backing made of stainless steel, one of the rare metals with which magnesium does not react. The Si and S polycrystalline targets were prepared by dusting the powdered crystals onto an adhesive backing to form a continuous coating. For the P target, we crushed small high-purity phosphorus granules and dusted the obtained powder as before on an adhesive backing. For Cl, due to safety reasons, we employed only compounds, namely NaCl and RbCl. The latter were prepared with the same technique as the one used for Si and S. All targets had a 20-mm-high$\times$5-mm-wide rectangular shape with thicknesses ranging from several μm to a few tenths of mm.

III. THEORY

A. Sudden approximation

In the incident particle (photons or electrons) high-energy limit, one may use the so-called sudden approximation [9], in which the atomic excitation is treated separately from the initial vacancy process. Experimental results of Carlson and Krause [3] and Carlson *et al.* [10], as well as theoretical predictions of Krause and Carlson [11], and Sachenko and Burtsev [12] indicate the validity of this approximation for atomic excitation following inner-shell vacancy production. Several calculations for rare-gas atoms in the sudden approximation are referred to in the paper of Mukoyama and Taniguchi [9], presenting results for the probabilities of atomic excitation as a result of vacancy production in the $1s$, $2s$, and $2p$ shells for elements with Z between 2 and 36 in the sudden approximation. These authors used nonrelativistic Hartree-Fock-Slater wave functions.

B. The multiconfiguration Dirac-Fock method

The multiconfiguration Dirac-Fock (MCDF) code of Desclaux and Indelicato [13–15] was used in this work to generate the wave functions. The MCDF method starts from a no-pair Hamiltonian, written in the following form [14,16,17]:

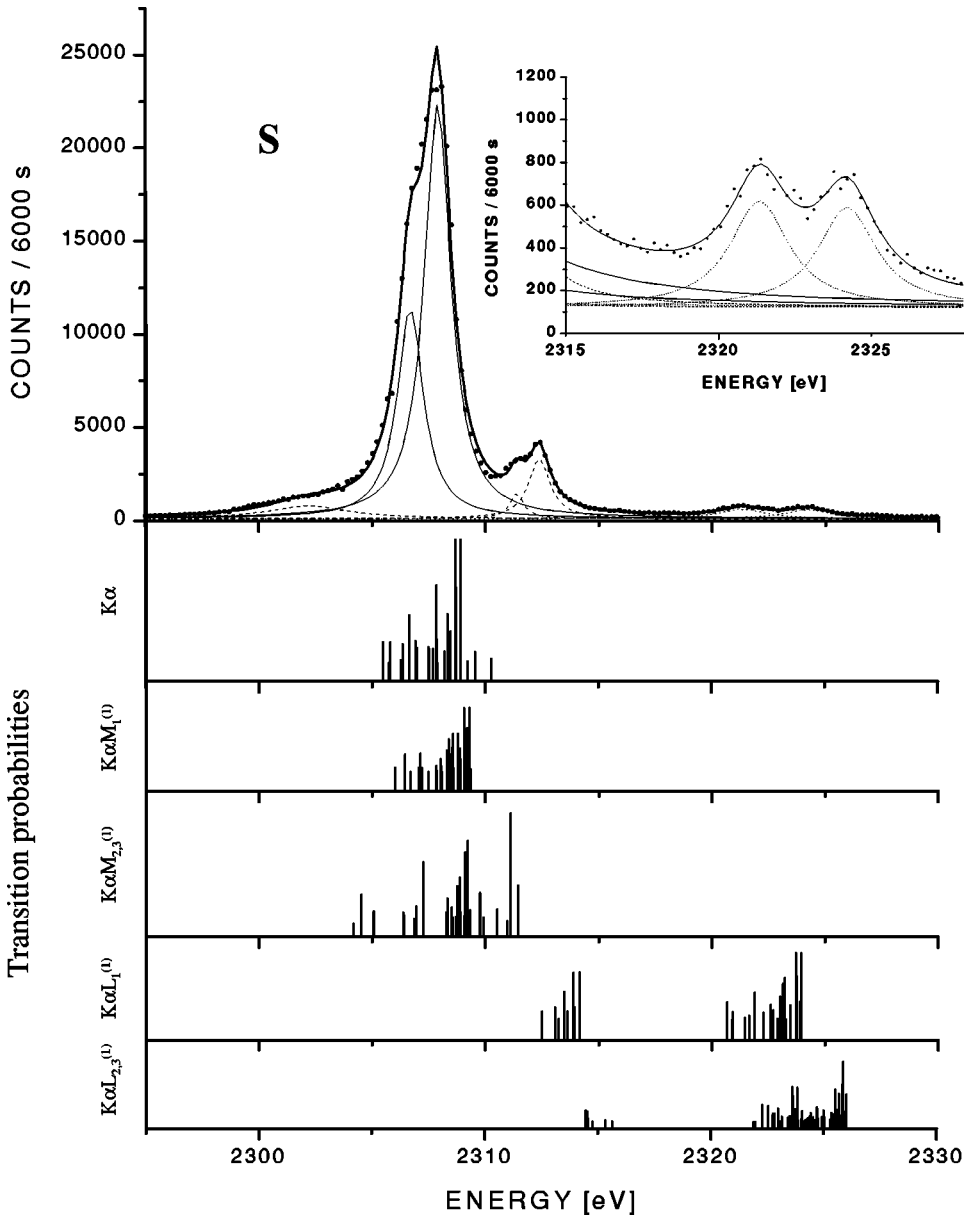

FIG. 1. High-resolution $K\alpha_{1,2}$ x-ray spectrum of sulfur. The *L*-satellite structure is shown enlarged in the inset. The dots correspond to the experimental data, the thick solid line to the total fit of the spectrum. The Lorentzians used to fit the diagram line and the *L* and *M* satellites are represented by thin solid lines, dotted lines, and dashed lines, respectively. The lower part of the figure shows the results of the MCDF calculations. The stick spectra represent the relative strengths of the components pertaining to the $2p$-$1s$ transition with, respectively, no spectator vacancy or one spectator vacancy in the M_1, $M_{2,3}$, L_1 or $L_{2,3}$ subshell. Each stick spectrum was normalized so that the sum of the transition probabilities is equal to one.

$$\mathcal{H}^{\text{nopair}}=\sum_{i=1}^{m}\mathcal{H}_{\text{D}}(r_i)+\sum_{i<j}\mathcal{V}(|\mathbf{r}_i-\mathbf{r}_j|). \tag{1}$$

$\mathcal{H}_{\text{D}}$ is an one-electron operator and $\mathcal{V}$ is an operator representing the two-body interaction

$$\mathcal{V}_{ij}=\Lambda_{ij}^{++}V_{ij}\Lambda_{ij}^{++}, \tag{2}$$

where, in the Coulomb gauge,

$$\mathcal{V}_{ij}=\frac{1}{r_{ij}}-\frac{\boldsymbol{\alpha}_i\cdot\boldsymbol{\alpha}_j}{r_{ij}}-\frac{\boldsymbol{\alpha}_i\cdot\boldsymbol{\alpha}_j}{r_{ij}}[\cos(\omega_{ij}r_{ij})-1]$$

$$+(\boldsymbol{\alpha}_i\cdot\boldsymbol{\nabla}_i)(\boldsymbol{\alpha}_j\cdot\boldsymbol{\nabla}_j)\frac{\cos(\omega_{ij}r_{ij})-1}{\omega_{ij}^2 r_{ij}}, \tag{3}$$

and $\Lambda_{ij}^{++}=\Lambda_i^+\Lambda_j^+$ is an operator projecting onto the one-electron positive continuum which avoids coupling the positive- and negative-energy continuum. We define $r_{ij}=|\mathbf{r}_i-\mathbf{r}_j|$ for the interelectronic distance, ω_{ij} for the energy of the exchanged photon between the electrons and $\boldsymbol{\alpha}_i$ the Dirac matrices ($\boldsymbol{\nabla}$ acts only on the r_{ij} and not on the following wave function).

The total wave function is calculated with the help of the variational principle. The total energy is the eigenvalue of the equation

$$\mathcal{H}^{\text{nopair}}\Psi_{\Pi,J,M}(r_1,\ldots,r_m)=E_{\Pi,J,M}\Psi_{\Pi,J,M}(r_1,\ldots,r_m), \tag{4}$$

where Π is the parity, **J** is the total angular momentum eigenvalue, and *M* is the eigenvalue of its projection on the *z* axis J_z. The MCDF method is defined by the particular choice of a trial function to solve Eq. (4) as a linear combination of configuration state functions (CSF)

$$|\Psi_{\Pi,J,M}\rangle=\sum_{\nu=1}^{n}c_\nu|\nu,\Pi,J,M\rangle. \tag{5}$$

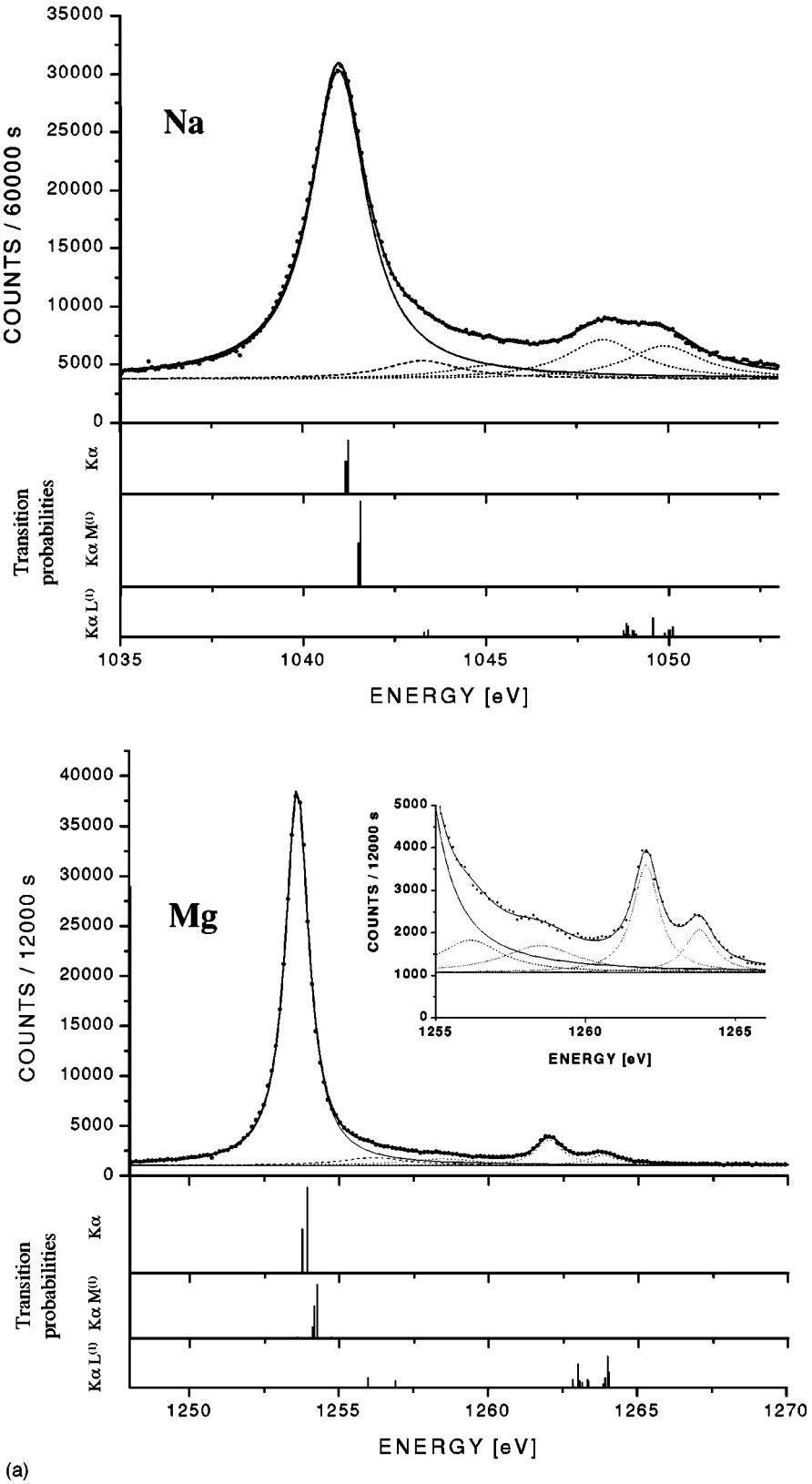

FIG. 2. High-resolution x-ray spectra of sodium (elemental Na target), magnesium, aluminum, silicon, phosphorus, and chlorine (NaCl target) with the corresponding MCDF stick spectra. For the fitted satellites, the same representation as in Fig. 1 is used.

The CSF are eigenfunctions of the parity Π, the total angular momentum $\mathbf{J}^2$, and its projection J_z. The CSF are antisymmetric products of one-electron wave functions expressed as linear combinations of Slater determinants of Dirac four-spinors

$$|\nu,\Pi,J,M\rangle = \sum_{i=1}^{N_\nu} d_i \begin{vmatrix} \psi_1^i(r_1) & \cdots & \psi^i(r_1) \\ \vdots & \ddots & \vdots \\ \psi_1^i(r_m) & \cdots & \psi_m^i(r_m) \end{vmatrix}. \quad (6)$$

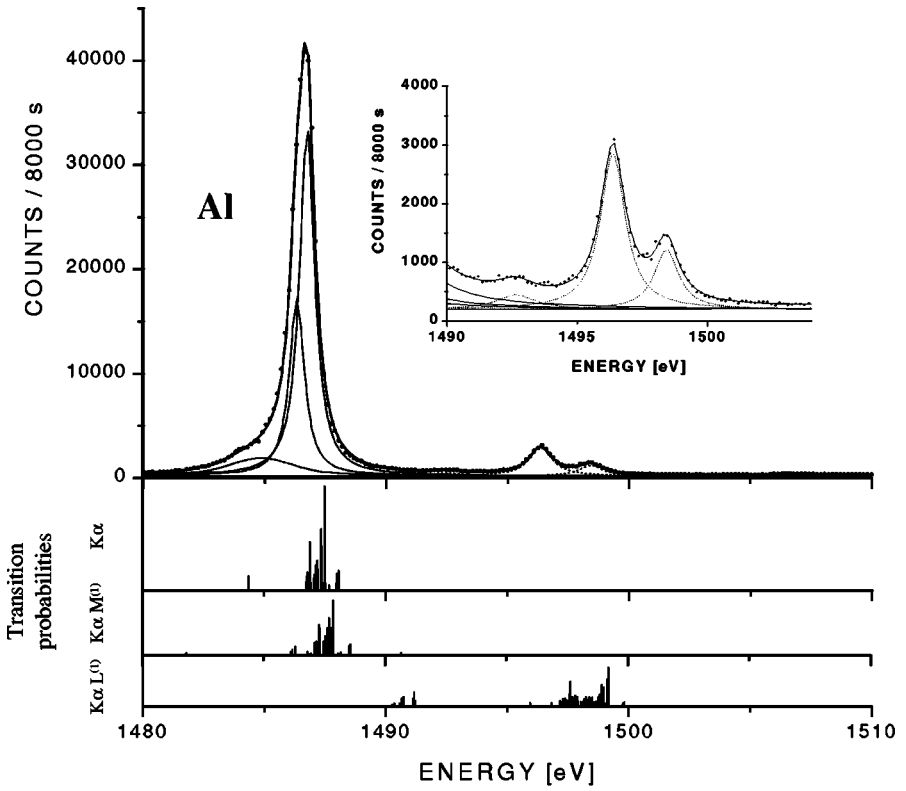

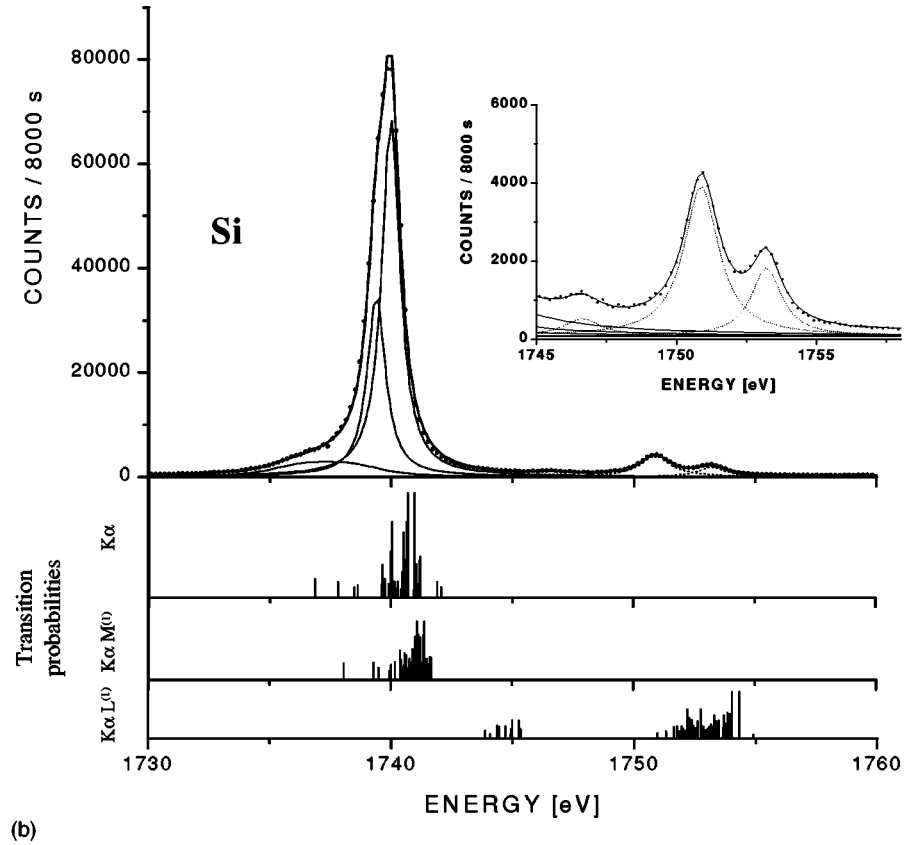

(b)

FIG. 2. (*Continued*.)

The d_i coefficients are obtained by requiring that the CSF are eigenstates of $\mathbf{J}^2$ and J_z. A variational principle provides the integro-differential equations to determine the radial wave functions and a Hamiltonian matrix that provides the mixing coefficients c_ν by diagonalization. Exact one-electron radiative corrections (self-energy and vacuum polarization) are added afterwards.

C. Calculations

We used relativistic MCDF wave functions in monoconfiguration for the neutral atom (initial state) and for the ion

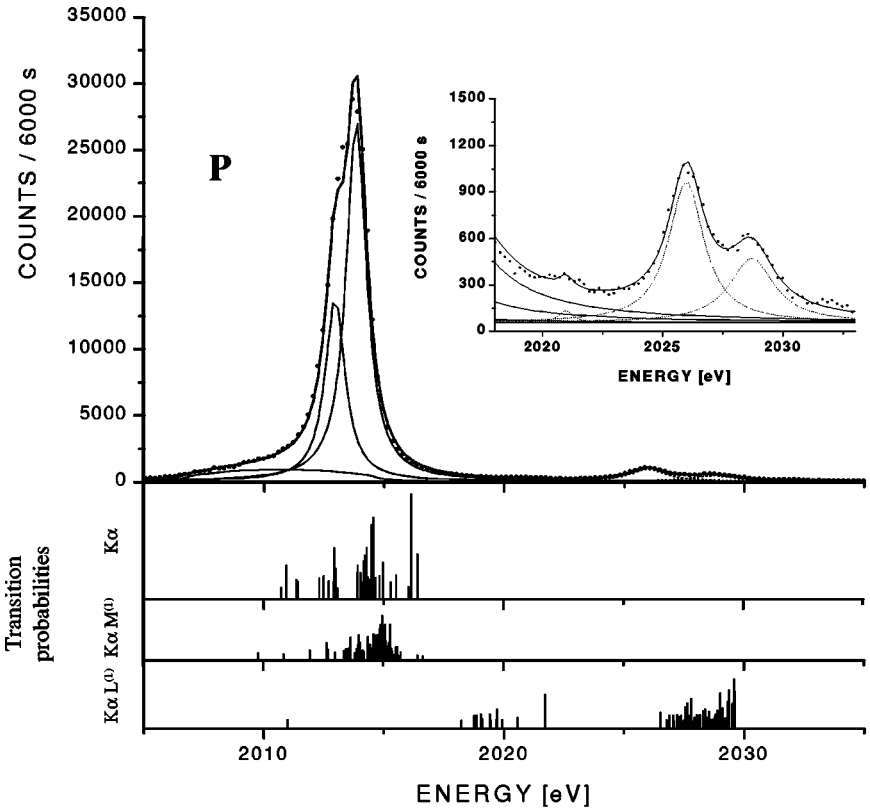

FIG. 2. (*Continued*.)

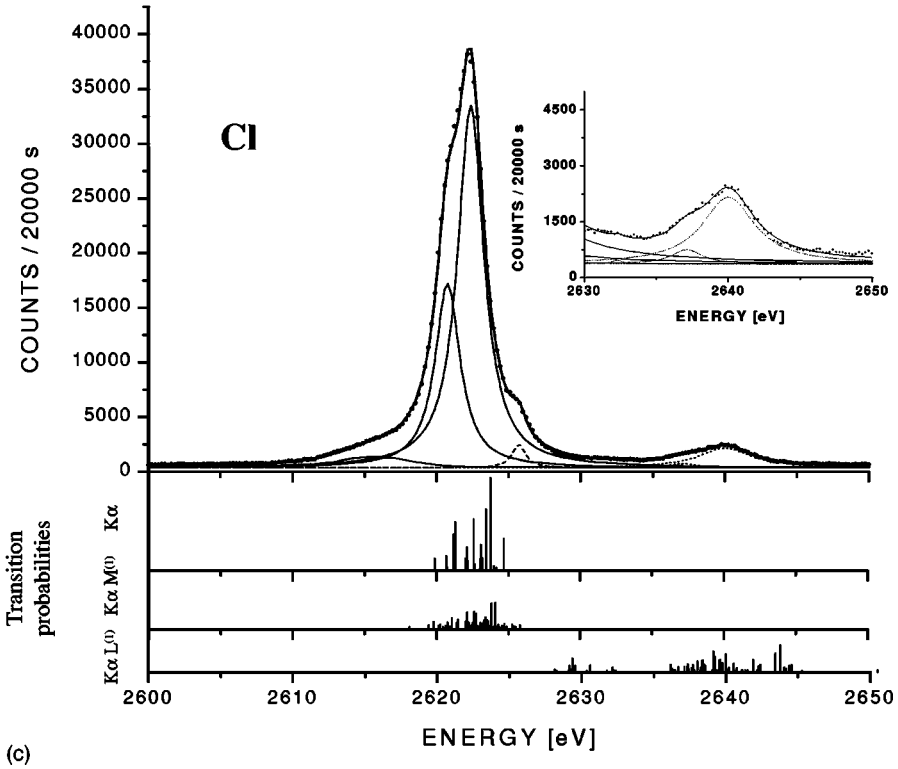

(c)

with a single 1*s* hole (final state). In the sudden approximation, the overlap between the initial and final wave functions gives the electron transition probability between those two states due to a sudden change in the atomic potential.

According to Carlson *et al.* [3] the probability for removing an electron from an orbital nlj, is given by

$$P_{nlj}=1-\left[\left|\int \psi'^{*}_{nlj}\psi_{nlj}d\tau\right|^{2}\right]^{N}-P_{F}, \tag{7}$$

where ψ_{nlj} and ψ'_{nlj} represent the electron wave functions of

the orbital nlj in the neutral atom and the ion with a single $1s$ vacancy, respectively, N is the number of electrons in the nl shell, and

$$P_F = \sum_{n'=1}^{x} \frac{NN'}{2j+1} \left| \int \psi'^{*}_{n'lj} \psi_{nlj} d\tau \right|^2 \tag{8}$$

with $n \neq n'$, N' being the number of electrons in the $n'l$ shell. x is the principal quantum number of the highest occupied state and thus P_F represents a correction introduced by the condition that the electron shake-up transitions to occupied levels are not physically allowed. The second term of Eq. (7) gives the probability that an electron initially in orbital nlj remains in an orbital with the same quantum numbers in the final state.

Many shake calculations are based on the relation (7). Depending on the scheme employed to compute the wave functions, the results vary somewhat. In the calculations performed with the code of Desclaux, the wave functions were calculated for all possible **J** values and the shake probability was then obtained from the weighted sum of all overlap integrals. Complementary calculations were performed within the same approach but using self-consistent Dirac-Fock wave functions computed in the energy average level (EAL) scheme with the code of Dyall [18]. As expected, the results of the two MCDF calculations were found to differ slightly. They are presented in Fig. 3 together with theoretical predictions from [9] based on nonrelativistic HFS (Hartree-Fock-Slater) wave functions.

IV. DATA ANALYSIS

The observed K x-ray spectra were analyzed by means of the least-squares-fitting computer program MINUIT [19], employing Lorentzian profiles to fit the diagram and satellite lines. Lorentz functions were chosen because the instrumental response of the von Hamos spectrometer operated in the slit geometry can be well reproduced by a Lorentz profile so that the convolution of the spectrometer response with the natural line shape of the x-ray transitions remains a Lorentzian. As each satellite line consists of many overlapping components, their complex shape was reproduced by several juxtaposed Lorentzians, whose centroid position, amplitude, and width were used as free-fitting parameters. The same held for those diagram transitions for which an asymmetric shape was observed resulting from unresolved M satellite structures and, for certain elements, from open valence subshells in the ground state.

In order to better understand the structure of the measured spectra, and in particular to assign properly the fitted satellite yields, MCDF (multiconfiguration Dirac-Fock) calculations based on the MSAL (modified special average level) version [20] of the GRASP code [18] were performed for all investigated elements. In each ''stick'' spectrum resulting from the MCDF calculations, the transition probabilities were scaled so that their sum is equal to one. MCDF predictions reproduce quite well the general trends of the experimental x-ray spectra and were therefore very useful for the qualitative interpretation of the observed structures. However, deviations from the experimental energies and intensities of the satellite components were observed, making questionable quantitative detailed comparisons.

To illustrate the method used for the data analysis, the fitted $K\alpha L^{(0,1)}$ x-ray spectrum of S is presented in Fig. 1. The first group of lines, centered around 2307 eV, corresponds principally to the $K\alpha_1$ and $K\alpha_2$ diagram transitions which were fitted with a single Lorentzian each. The intensity ratio $I(K\alpha_2):I(K\alpha_1)$ and the energy difference $E(K\alpha_1)-E(K\alpha_2)$ were kept fixed in the fitting procedure at the values of 0.506 and 1.2 eV quoted in Refs. [21] and [8], respectively. As indicated by the MCDF calculations, a significant part of the fitted intensity is due to overlapping M satellite components.

The double bump structure above 2320 eV which was fitted with two Lorentzians (dotted lines) is clearly due to L satellites. The first peak (called $K\alpha_3$ in the literature) originates predominantly from K-$L_{2,3}$ transitions with one additional spectator hole in the L_1 subshell while the second one ($K\alpha_4$) arises mainly from the radiative decay of $1s^{-1}2p^{-1}$ double-hole states. Furthermore, the $K\alpha L_1^{(1)}$ and $K\alpha L_{2,3}^{(1)}$ stick spectra show that there is a third group of L satellites below and around 2315 eV. However, these components could not be fitted because they are completely hidden by the overlapping M-satellite structure. Theory predicts that the probability to eject an electron from the $2s$ subshell as a result of the sudden production of a K hole is about 30 times smaller than the probability to eject an electron from the $3p$ subshell. As a consequence, the rather strong doublet occuring at 2312 eV cannot indeed be explained by the lower group of the $K\alpha L_1^{(1)}$ satellites but is very certainly due to the higher-energy components of the $K\alpha M_{2,3}^{(1)}$ satellite group. Similarly, the shoulder appearing on the left side of the diagram lines stems probably from the lower-energy components of the $K\alpha M_{2,3}^{(1)}$ group. This excess of intensity around about 2302 eV cannot indeed be attributed to K-LM radiative Auger (RAE) transitions [6,22], because the latter are expected to occur below 2287 eV (edge of the K-$L_3M_3\,{}^1P_1$ transition, the K-LM RAE transition of highest energy as indicated by Larkins's tables [23]).

As it can be seen from Fig. 1, the diagram lines, which were fitted with two Lorentzians, consist in fact of many components whose energies spread over about 5 ev. This is related to the open $3p$ subshell of S in the ground state. Depending on the coupling between the two $3p$ vacancies with the $1s$ hole in the initial state and with the $2p$ hole in the final state, several different initial and final states do indeed exist which give rise to numerous transitions as shown in the stick spectrum labeled $K\alpha$.

MCDF calculations concerning $K\alpha L^{(1)}M^{(1)}$ transitions (i.e., $2p$-$1s$ transitions with one spectator vacancy in the L shell plus one in the M shell) were also performed. The results were found to be very similar to those corresponding to the $K\alpha L^{(1)}$ transitions. As a consequence, their contribution to the observed x-ray spectrum is implicitly included in the three Lorentzians employed to fit the L-satellite structures.

Finally, for sulfur the $X_{K\alpha L^{(1)}}$:$X_{K\alpha L^{(0)}}$ yield ratio was computed by taking for $X_{K\alpha L^{(0)}}$ the sum of the yields of the

TABLE II. Correction factors and x-ray intensity ratios.

Z	Target	Correction factor	$X_{K\alpha_4}:X_{K\alpha_3}$	$X_{K\alpha L^{(1)}}:X_{K\alpha L^{(0)}}(\%)$ Present	$X_{K\alpha L^{(1)}}:X_{K\alpha L^{(0)}}(\%)$ Earlier
11	Na	0.994	0.85 ± 0.02	27.1 ± 0.3	19.6 [a] [31]
11	NaCl	0.992	1.00 ± 0.08	25.6 ± 0.5	18.9 [a] [31]
12	Mg	1.018	0.39 ± 0.01	11.4 ± 0.1	13.9 ± 0.6 [b] [32] 16.1 ± 0.7 [a] [30]
13	Al	1.015	0.382 ± 0.009	7.80 ± 0.08	10.2 ± 0.5 [a] [30]
14	Si	0.994	0.452 ± 0.006	5.72 ± 0.03	11.4 [a] [33]
15	P	0.990	0.47 ± 0.01	3.40 ± 0.06	
16	S	0.991	0.94 ± 0.02	2.57 ± 0.03	
17	RbCl	0.987	5.5 ± 0.6	4.9 ± 0.1	
17	NaCl	0.990	2.1 ± 0.1	4.5 ± 0.2	

[a]Excitation mode: electrons.

[b]Excitation mode: photons (Rh x-ray tube, 40 kV, 40 mA).

five Lorentzians represented by solid lines (diagram transitions) and dashed lines ($K\alpha M^{(1)}$ satellites) and for $X_{K\alpha L^{(1)}}$ the sum of the yields of the two Lorentzians depicted with dotted lines ($K\alpha L^{(1)}$ satellites, $K\alpha L^{(1)}M^{(1)}$ components included).

A similar analysis was performed for the other investigated elements, namely Na, Mg, Al, Si, P, and Cl. The corresponding fitted $K\alpha L^{(0,1)}$ x-ray spectra are presented in Fig. 2 with the associated $K\alpha$, $K\alpha L^{(1)}$, and $K\alpha M^{(1)}$ MCDF stick spectra. Note that for Na whose ground state is characterized by a single $3s$ vacancy and especially for Mg which has only closed subshells in the ground state, the numbers of components in the stick spectra are considerably smaller than for other elements. For Cl, the bump occurring on the high-energy flank of the diagram line originates from the upper group of M satellites as in the case of S.

Although the energy differences between the diagram and L-satellite lines are small (10–20 eV), the dependence on the photon energy of the x-ray absorption in the target, crystal reflectivity and solid angle of the spectrometer were probed and their effect on the $X_{K\alpha L^{(1)}}:X_{K\alpha L^{(0)}}$ x-ray yield ratios checked. The corrections were found to be small (1% - 2%) and to partly cancel each other. The total correction factors, the intensity ratios $X(K\alpha_4):X(K\alpha_3)$ and the corrected $X_{K\alpha L^{(1)}}:X_{K\alpha L^{(0)}}$ yield ratios are presented in Table II. For Na and Cl, which were measured with two different targets each, results of both measurements are given. Experimental data from other groups, if existing, are also quoted.

V. RESULTS AND DISCUSSION

A. *L*-shell rearrangement

The measured L-satellite yields reflect the distribution of the spectator holes at the moment of the K x-ray emission and not the initial distribution following the $1s$ photoionization which has to be known for the determination of the shake probabilities. Processes such as LMM Auger and L radiative transitions occurring prior to the K x-ray emission can indeed modify the number of spectator holes created by the shake process. In order to deduce the primary vacancy distributions from the observed satellite intensities, we employed the statistical method described in the Appendix of Ref. [1].

The probability W_p for a process, modifying the number of holes in the subshell X_i, to occur before the $K^{(1)}X_i^{(1)}$ doubly ionized state decays is given by

$$W_p=\frac{\Gamma_p}{\Gamma_K+\Gamma_{X_i}}, \tag{9}$$

where Γ_p is the transition width of this particular process and Γ_K and Γ_{X_i} are the total widths of the K shell and the subshell X_i.

For $KL^{(1)}$ satellites of the studied elements the electron rearrangement is governed by LMM Auger transitions and L radiative transitions, which both decrease the number of L vacancies by one. If one neglects the triply ionized states $K^{(1)}L^{(2)}$ which are poorly populated by photoinduced shake processes, the diagram and satellite x-ray emission yields $X_{K\alpha L^{(n)}}$ are related to the initial vacancy yields $I_{K^{(1)}L^{(n)}}$ by the following equations:

$$X_{K\alpha L^{(0)}}=(I_{K^{(1)}L^{(0)}}+R_L I_{K^{(1)}L^{(1)}})\,\omega_{K\alpha L^{(0)}}, \tag{10}$$

$$X_{K\alpha L^{(1)}}=(I_{K^{(1)}L^{(1)}}-R_L I_{K^{(1)}L^{(1)}})\,\omega_{K\alpha L^{(1)}}, \tag{11}$$

where R_L is a scaling factor describing the electron rearrangement and $\omega_{K\alpha L^{(n)}}$ the partial K-shell fluorescence yield of the transition $K\alpha$ with n spectator holes in the L shell. The initial vacancy yield ratio can then be deduced from the system of equations (10) and (11),

$$\frac{I_{K^{(1)}L^{(1)}}}{I_{K^{(1)}L^{(0)}}}=\frac{\left(\frac{X_{K\alpha L^{(1)}}}{X_{K\alpha L^{(0)}}}\right)\left(\frac{\omega_{K\alpha L^{(0)}}}{\omega_{K\alpha L^{(1)}}}\right)}{1-R_L\left[1+\left(\frac{X_{K\alpha L^{(1)}}}{X_{K\alpha L^{(0)}}}\right)\left(\frac{\omega_{K\alpha L^{(0)}}}{\omega_{K\alpha L^{(1)}}}\right)\right]}. \tag{12}$$

Taking into consideration that L_iL_jM Coster-Kronig transitions do not modify the number of L holes, one obtains from Eq. (9) the following expression for the rearrangement factor of the subshell L_i:

TABLE III. Weighting factors of the L_i subshells used in the rearrangement calculations.

Elements	w_{L_1}	w_{L_2}	w_{L_3}
Na	0.115	0.299	0.586
Mg	0.091	0.306	0.603
Al	0.098	0.269	0.633
Si	0.112	0.285	0.603
P	0.114	0.297	0.589
S	0.123	0.271	0.606
Cl	0.134	0.268	0.598

$$R_{L_i}=\frac{\Gamma_{L_i}-\sum_j \Gamma_{L_iL_jM}}{\Gamma_K+\Gamma_{L_i}}. \tag{13}$$

The total *L*-shell rearrangment factor R_L can be written as the weighted sum of the coefficients R_{L_i},

$$R_L=\sum_i w_{L_i}R_{L_i}=\sum_i w_{L_i}\frac{\Gamma_{L_i}}{\Gamma_K+\Gamma_{L_i}}\left(1-\sum_j f_{ij}\right), \tag{14}$$

where f_{ij} represent the relative Coster-Kronig yields and w_{L_i} the weighting factors of the subshells L_i. As L_2L_3M Coster-Kronig transitions are energetically forbidden for the investigated elements, only the coefficients f_{12} and f_{13} need to be considered. They were taken from Ref. [24]. The weighting factors w_i are proportional to the numbers of initial holes in the subshells L_i, i.e., to the subshell shake probabilities. The latter were computed within the sudden approximation model by means of the method described in Sec. III. The so-obtained weighting factors w_i are given in Table III. The natural widths Γ_K and Γ_{L_i} were taken from Ref. [25] and the fluorescence yields $\omega_{K\alpha L^{(0)}}$ from [26]. The fluorescence yields $\omega_{K\alpha L^{(1)}}$ were deduced from a linear interpolation of the values quoted in [27]. The rearrangement factors, fluorescence yield ratios, and initial vacancy yield ratios obtained for the different targets are summarized in Table IV.

B. Shake probabilities

If we assume that there is no correlation between the ejected electrons, the primary vacancy yields $I_{K^{(1)}L^{(h)}}$ ($h=0,1$) can be written as follows:

$$I_{K^{(1)}L^{(h)}}\sim\sigma_K^{photo}\binom{8}{h}p_L^h(1-p_L)^{8-h} \tag{15}$$

where σ_K^{photo} is the photoionization cross section, p_L the average *L*-shell shake probabitity per electron, and $\binom{8}{h}$ the binomial coefficient. Using Eq. (15), one can express p_L as a function of the initial vacancy yield ratio

$$i_L:=\frac{I_{K^{(1)}L^{(1)}}}{I_{K^{(1)}L^{(0)}}}=\frac{8p_L}{1-p_L},\quad p_L=\frac{i_L}{8+i_L}. \tag{16}$$

The probability for the ionization via shakeoff plus shakeup processes of at least one electron from the *L* shell is then given simply by

$$P_L=8p_L. \tag{17}$$

Introducing in Eq. (16) the initial vacancy yield ratios quoted in Table IV, one obtains from Eq. (17) the experimental *L*-shell shake probabilities P_L listed in Table V. The latter are compared in Fig. 3 to the results of the calculations performed within the sudden approximation model with the above-mentioned wave functions.

If one considers at first the pure elemental targets, one can see from Fig. 3 that the theoretical sudden approximation calculations reproduce satisfactorily the experimental results, except for the lightest element (Na). Actually, the three calculations give very similar results and all of them underestimate by a factor of about 1.5 the experimental shake probability of Na. An explanation for the observed discrepancy may reside in the fact that the theoretical calculations are based on the free atom model and are thus not fully adequate for solid targets in which solid-state effects may affect the shake probabilities. In our opinion, however, solid state effects cannot explain solely the deviations found for Na since for Ne theory predicts a shake probability of 18% which is also markedly smaller than the experimental value of 29%

TABLE IV. Rearrangement factors R_L, partial fluorescence yield ratios ω_L, x-ray yield ratios x_L, and initial vacancy yield ratios i_L for the investigated targets ($\omega_L=\omega_{K\alpha L^{(0)}}:\omega_{K\alpha L^{(1)}}$, $x_L=X_{K\alpha L^{(1)}}:X_{K\alpha L^{(0)}}$, $i_L=I_{K^{(1)}L^{(1)}}:I_{K^{(1)}L^{(0)}}$).

Z	Target	R_L	ω_L	x_L (%)	i_L (%)
11	Na	0.059±0.043	0.911	27.1±0.3	26.6±2.2
11	NaCl	0.059±0.043	0.911	25.6±0.5	25.2±2.0
12	Mg	0.076±0.036	0.902	11.4±0.1	11.2±0.9
13	Al	0.087±0.033	0.897	7.80±0.08	7.71±0.49
14	Si	0.094±0.030	0.898	5.72±0.03	5.70±0.35
15	P	0.117±0.027	0.900	3.40±0.06	3.48±0.21
16	S	0.132±0.026	0.897	2.57±0.03	2.67±0.16
17	RbCl	0.144±0.025	0.892	4.9±0.1	5.1±0.3
17	NaCl	0.144±0.025	0.892	4.5±0.2	4.7±0.4

TABLE V. Experimental *L*-shell shake probabilities.

Target	Na	**Na**Cl	Mg	Al	Si	P	S	Rb**Cl**	Na**Cl**
P_L (%)	26(2)	24(2)	11.0(9)	7.6(5)	5.6(3)	3.5(2)	2.6(2)	5.1(3)	4.7(4)

$\pm 3\%$ deduced from the x-ray yield ratio ($32\% \pm 3\%$) quoted for this rare gas in Ref. [28].

In the sudden approximation approach, the atomic excitation is treated separately from the initial vacancy production to which no reference is required except that the resulting change in the atomic potential due to the alteration in electron screening must be fast enough. From a study of the double ionization induced in Ne and Ti targets bombarded by photons and electrons, Krause [29] found that the breakdown point of the sudden approximation appears to occur at

$$\eta_{KL} = \frac{E_{ph,e} - B_K - B_L}{B_L} \approx 10, \tag{18}$$

where the numerator represents the excess energy of the incident particle ($E_{ph,e}$) over the ionization energy of the *K*-shell electron (B_K) plus the ionization energy of the shaken *L* electron (B_L) which refers to an ion with a hole in the *K* shell. The values of the parameter η_{KL} corresponding to the photoionization processes studied in the present paper are presented in Table I. They are all much bigger than 10. A comparison of our experimental results with sudden approximation predictions is thus meaningful. In particular, the average bremsstrahlung energy used for the Na $K^{(1)}L^{(1)}$ double excitation lies far above the break point of the sudden approximation and cannot therefore account for the observed discrepancy.

The x-ray yield ratios $K\alpha L^{(1)}$:$K\alpha L^{(0)}$ quoted in the last column of Table II were obtained mainly from electron bombardment and thus cannot be compared directly to our results. In the electron case, there is indeed a significant contribution to the $K^{(1)}L^{(1)}$ double ionization which arises from the simultaneous direct Coulomb excitation of two electrons by the charged projectile. As shown in Table II for Mg, which was measured earlier by means of both photon [32] and electron bombardment [30], one can see that the photon excitation gives a result which is smaller than the one corresponding to the electron excitation. In this context it is intriguing to note that the result of an earlier measurement concerning sodium [31], which was performed with 6 keV electrons, is smaller than our result obtained by photoionization. No explanation was found for this observation. For Mg, there is a discrepancy between our result and the one quoted in Ref. [32]. This discrepancy cannot be explained by the difference of the target thickness (0.01 mm in the present work, 4.0 mm in [32]) because in both experiments the x-ray yields were corrected for the self-absorption effect. Although there is no information about the data analysis in Ref. [32], we believe that the reason of the discrepancy resides in the interpretation of the observed satellite structures. We have indeed fitted the excess of intensity observed around 1256 eV with one Lorentzian (see Fig. 2, inset of the Mg spectrum) which was attributed to *M* satellites according to MCDF predictions. If this Lorentzian is included in the *L*-satellite components, our $K\alpha L^{(1)}$:$K\alpha L^{(0)}$ yield ratio increases to a value which is consistent with the result quoted in [32].

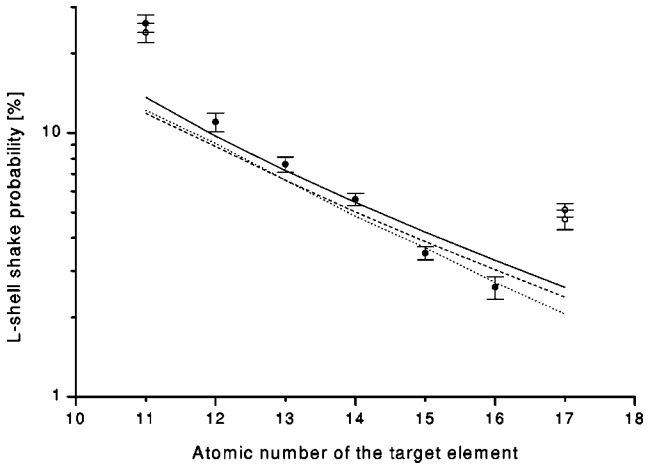

FIG. 3. Total *L*-shell shake probabilities. Results corresponding to elemental targets are represented by full circles (●), those obtained with compound targets by open circles (○). The solid and dotted lines represent the results of our MCDF calculations performed with the Dyall's and Desclaux's codes, respectively, while the dashed line corresponds to theoretical predictions by Mukoyama [9].

As mentioned above, the satellite intensities are sensitive to the crystal environment of the atoms and ions. This statement is supported by numerous experimental results. For instance, Baun and Fisher [34] have shown that an important change in the $K\alpha_4$ to $K\alpha_3$ yield ratio and in the total peak intensity of the *L* satellites occurs in magnesium, aluminum, and silicon when these elements oxidize. Similar observations were done for the *M* satellites of heavier elements. For example, measurements of the Cl $K\beta_{1,3}$ spectra in the chlorides [35] evinced fluctuations in the *M* satellite yields up to a factor of 1.4. In addition, it was found by Kawai [36–38] that in chlorides the relative *M*-satellite intensity decreases almost linearly with the electronegativity of the element involved in the compound. Actually, a large electronegativity of the compound element indicates that the $3p$ electrons of chlorine are partly delocalized or that the bonding in the chloride is predominantly covalent. This delocalization leads to a diminution of the electronic screening in the chlorine atoms, i.e., to an enhancement of the effective binding energy of the electrons, which in turn results in a decrease of the *M*- and *L*-shell shake probabilities. If the electronegativity is on the contrary small, the bonding character is predominantly ionic, i.e., the Cl $3p$ electrons are more localized and, as a consequence, the shake probabilities are increased. Rubidium and sodium have an electronegativity of 0.8 and

0.9, respectively, which are both small with respect to that of chlorine (3.0). As expected the shake probabilities of Cl observed with the RbCl ($5.1\% \pm 0.3\%$) and NaCl ($4.7\% \pm 0.4\%$) targets are similar but both higher than the one predicted by theory for the pure element [the three theoretical predictions for chlorine are 2.6% (Dyall code), 2.1% (Desclaux code), and 2.4% (Mukoyama)]. The ionic character of NaCl which leads to an increase of the shake probability of Cl has the opposite influence on the shake probability of Na. Due to the delocalization of the 3*s* electron of Na, the electronic screening in the sodium atoms embedded in the NaCl crystal diminishes, which leads to an increase of the binding energies of the 2*s* and 2*p* electrons, i.e., to the observed decrease of the *L*-shell shake probability from $26\% \pm 2\%$ (Na) to $24\% \pm 2\%$ (NaCl).

Solid state and chemical effects are also expected to modify slightly the energies and transition probabilities of the components pertaining to the same satellite. As a consequence, the line shapes of the observed satellites and in particular the $K\alpha_4$:$K\alpha_3$ yield ratios must reflect the influence of the neighbor atoms or ions. As shown in Table II, the $K\alpha_4$ to $K\alpha_3$ yield ratios found in the present study for pure elemental targets decrease first from 0.85 (Na) to 0.38 (Al) and then increase again up to 0.94 (S). A quadratic polynomial interpolation of the six ratios obtained for the elements Na to S results for pure Cl in a value of about 1.4 which is indeed quite different than the values obtained from the fits of the Cl spectrum corresponding to the NaCl target (value of 2.1) and RbCl target (value of 5.5). Similarly, the $K\alpha_4$ to $K\alpha_3$ yield ratio obtained from the analysis of the Na spectrum measured with the NaCl target is larger (1.0) than the one deduced from the measurement with the pure Na target (0.85). A qualitative interpretation of these findings is, however, far beyond the objectives of the present study and needs further and more detailed theoretical investigations.

ACKNOWLEDGMENTS

This work was partly supported by the Swiss National Science Foundation and the Polish Committee for Scientific Research (KBN), Grant No. PO3B 019 16.

[1] J.-Cl. Dousse and J. Hoszowska, Phys. Rev. A **56**, 4517 (1997).
[2] T. Åberg, Phys. Rev. **156**, 35 (1967).
[3] T.A. Carlson and M.O. Krause, Phys. Rev. A **140**, 1057 (1965).
[4] T.A. Carlson and C.W. Nestor, Jr., Phys. Rev. A **8**, 2887 (1973).
[5] J. Hoszowska, J.-Cl. Dousse. J. Kern, and Ch. Rhême, Nucl. Instrum. Methods Phys. Res. A **376**, 129 (1996).
[6] A. Mühleisen, M. Budnar, J.-Cl. Dousse, J. Hoszowska, and Z.G. Zhao, X-Ray Spectrom. **27**, 337 (1998).
[7] P.-A. Raboud, J.-Cl. Dousse, J. Hoszowska, and I. Savoy, Phys. Rev. A **61**, 012507 (2000).
[8] J.A. Bearden, Rev. Mod. Phys. **39**, 78 (1967).
[9] T. Mukoyama and K. Taniguchi, Phys. Rev. A **36**, 693 (1987).
[10] T.A. Carlson, W.E. Moddeman, and M.O. Krause, Phys. Rev. A **1**, 1406 (1970).
[11] M.O. Krause and T.A. Carlson, Phys. Rev. **158**, 18 (1967).
[12] V.P. Sachenko and E.V. Burtsev, Izv. Akad. Nauk SSSR, Ser. Fiz. 965 (1967) [Bull. Acad. Sci. USSR, Phys. Ser. **31**, 980 (1968)].
[13] J.P. Desclaux, Comput. Phys. Commun. **9**, 31 (1975).
[14] J.P. Desclaux, *Relativistic Multiconfiguration Dirac-Fock Package* (STEF, Cagliari, 1993), Vol. A.
[15] P. Indelicato, Phys. Rev. Lett. **77**, 3323 (1996).
[16] I.P. Grant, H.M. Quiney, Adv. At. Mol. Phys. **23**, 37 (1988).
[17] P. Indelicato, Phys. Rev. A **51**, 1132 (1995).
[18] K.G. Dyall *et al.*, Comput. Phys. Commun. **55**, 425 (1989).
[19] F. James and M. Roos, Comput. Phys. Commun. **10**, 343 (1975).
[20] M. Polasik, Phys. Rev. A **52**, 227 (1995).
[21] E. Storm and H.I. Israel, Nucl. Data Tables **7**, 565 (1970).
[22] Ch. Herren and J.-Cl. Dousse, Phys. Rev. A **56**, 2750 (1997) and references therein.
[23] F.P. Larkins, At. Data Nucl. Data Tables **20**, 313 (1977).
[24] E.J. McGuire, Phys. Rev. A **3**, 587 (1971).
[25] J.L. Campbell, T. Papp, X-Ray Spectrom. **24**, 307 (1995).
[26] M.O. Krause and J.H. Oliver, J. Phys. Chem. Ref. Data **8**, 307 (1979).
[27] T.W. Tunnel and C.P. Bhalla, Phys. Lett. **86A**, 13 (1981).
[28] R.E. LaVilla, Phys. Rev. A **4**, 476 (1971).
[29] M.O. Krause, J. Phys. (Paris), Colloq. **10 32**, C4-67 (1971).
[30] E. Mikkola, O. Keski-Rakkonen, J. Lahtinen, and K. Reinikainen, Phys. Scr. **28**, 188 (1983).
[31] O. Keski-Rahkonen, K. Reinikainen, and E. Mikkola, Phys. Scr. **28**, 179 (1983).
[32] K. Parthasaradhi *et al.*, Nucl. Instrum. Methods Phys. Res. A **255**, 54 (1987).
[33] S.N. Soni, J. Phys. B **31**, 1695 (1998).
[34] W.L. Baun and D.W. Fisher, in *Advances in X-Ray Analysis*, edited by W.M. Mueller, G.R. Mallet, and M.J. Fay (Plenum Press, Inc., New York, 1965), Vol. 8, p. 371.
[35] E.E. Vainshtein, L.N. Mazalov, and V.G. Zyryanov, Fiz. Tverd Tela (Leningrad) **7**, 1099 (1965) [Sov. Phys. Solid State **7**, 882 (1965)].
[36] J. Kawai, C. Satoko, K. Fujisawa, and Y. Gohshi, Phys. Rev. Lett. **57**, 988 (1986).
[37] J. Kawai, C. Satoko, K. Fujisawa, and Y. Gohshi, Spectrochim. Acta, Part B **42B**, 729 (1987).
[38] J. Kawai, C. Satoko, and Y. Gohshi, Spectrochim. Acta, Part B **42B**, 745 (1987).